Original scientific paper

Walnut (*Juglans regia* L.) fruit septum alcoholic extract as corrosion inhibitor for Fe B500B steel bars in mixed acidic solution

Alketa Lame✉, Muhamed Farruku, Efrosini Kokalari, Klodian Xhanari, Nensi Isak, Kledi Xhaxhiu and Alma Shehu

Faculty of Natural Sciences, University of Tirana, Boulevard "Zogu I'', 1001, Tirana, Albania

Corresponding author: ✉*alketa.lame@fshn.edu.al*

Abstract

*The corrosion inhibition performance of the walnut fruit (*Juglans regia *L.) septum alcoholic extract for Fe B500B steel bars in a mixed acidic solution (H_2SO_4/HCl) is reported. Weight loss, potentiodynamic polarization, and electrochemical impedance spectroscopy measurements were performed at 298 to 318 K, with the addition of various extract concentrations. Results showed the maximum corrosion inhibition efficiency of 86.99 % for 300 mg L^{-1} extract added. The extract acts as a mixed-type inhibitor, predominantly affecting the anodic side, following Flory-Huggins adsorption isotherm. Thermodynamic analysis indicated an endothermic process with both chemisorption and physisorption on the steel bar surface. Surface characterization was conducted using ATR-FTIR, UV-vis and SEM techniques to prove the adsorption of the inhibitor molecules on the steel bar surface. Also, a possible adsorption mechanism of inhibitor molecules was proposed.*

Keywords

Green corrosion inhibitor, corrosion rate; inhibition efficiency, Flory-Huggins isotherm, inhibitor adsorption mechanism

Introduction

Corrosion is an issue that costs economies billions of dollars worldwide [1]. Several techniques are used to mitigate corrosion, such as materials selection and isolation, design improvement, environment modification, *etc*. Different kinds of carbon steels used as reinforcements in constructions are susceptible to corrosion in aggressive environments. It is known that concrete with a basic media protects all types of carbon steel. The problem arises when concrete is damaged due to various chemical or physical causes. In contact with concrete, an aggressive environment migrates through the cracks on the surface of the reinforcement. Such aggressive environments include acid rain containing chloride ions in coastal urban industrial areas or acidic solutions used for pickling metals. According to the paper published by C. J. Brown and D.R. Olsen [2], *"Pickling is, and likely will remain, very much an art"*. Based on this paper, adding H_2SO_4 to HCl (traditional

pickling) increases the pickling rate. Furthermore, the inhibitors used to avoid attack in HCl pickling remain effective with mixed acids. All of these are the impetus of the scientific motivation to use a mixture of 0.5 M H_2SO_4/0.5 M HCl as an aggressive acidic environment (blank solution), which provides both the acidic environment with chloride ions and the corrosion situation during the pickling process. Both H_2SO_4 and HCl are strong corrosive acids [3,4].

Changing the environment using different additives as corrosion inhibitors is an effective solution to mitigate corrosion. Corrosion inhibitors are generally grouped into inorganic, organic, and environmentally friendly compounds extracted from plants [5-9]. Different parts of the plants have been extracted, such as bark, roots, seeds, fruit peels, and leaves [10-14]. The corrosion-protective properties of these extracts are attributed to flavonoids, phenolic compounds, tannins, *etc*. These active compounds added to the corrosive medium protect metals from corrosion due to heteroatoms such as N, O, as well as double bonds and aromatic rings, capable of adsorbing on the metal surface physically or chemically [15,16].

The high inhibition efficiency was previously reported for the extracts obtained from different parts of *Juglans regia* L, such as leaves, green husk, and walnut shell, in the corrosion of carbon steel, mild steel, and aluminum in aggressive media [17-21]. Several scientific publications were reported on the pharmaceutical and medical uses of the septum extract of the walnut fruit, thanks to its anti-inflammatory and antimicrobial properties. These properties are due to the presence of active compounds such as gallic acid, catechin, isoquercitrin, quercitrin, *etc.* [22,23]. The reason for selecting walnut septum extract as a corrosion inhibitor is the presence of compounds mentioned above and the low cost of this recyclable material in the fruit processing industry. These are the genesis for the design of the walnut fruit septum extract as an inhibitor against corrosion of Fe B500B steel bars in the acidic mixture (0.5 M H_2SO_4/0.5 M HCl).

The corrosion rate of the Fe B500B samples was evaluated using the weight loss method, potentiodynamic polarization, and electrochemical impedance spectroscopy (EIS). The measurements were carried out at room temperature with and without the addition of different concentrations of the extract and for the optimum concentration at 298 to 318 K range. Adsorption isotherms were used to find the type of adsorption on the metal solution interface. The activation energy was determined with the Arrhenius-type dependence. The walnut fruit septum extract was characterized by FTIR and UV-vis techniques. Scanning electron microscope (SEM) was used to investigate the surface morphology of the Fe B500B samples for blank and optimum concentration of the solution after 100 h of immersion in the 298 to 318 K temperature range.

Experimental

Preparation and characterization of the walnut fruit septum extract

The walnut fruit septum was obtained from domestic production in Albania and dried at 40 °C for 5 days. The dried walnut fruit septum was ground in a blender and then extracted for 24 h in 70 % ethanol under reflux at 298 K. The extract was filtered and stored at 277 K. HPLC-DAD was used to confirm the presence of gallic acid, catechin, isoquercitrin, and quercitrin which are the main compounds present in walnut septum extract as previously reported [22], and suitable for use as corrosion inhibitors.

Solution preparation

The mixed acidic corrosive medium (0.5 M H_2SO_4/0.5 M HCl) was prepared by diluting the 37 % HCl and 96 % H_2SO_4 solutions provided by Sigma Aldrich. The concentration of the extract was

calculated based on the difference of the dried plant mass before and after extraction divided by the volume of the solvent after reflux. The brown walnut fruit septum extract was added to the corrosive solution in the concentration range of 100 to 300 mg L^{-1} (*i.e.* 100, 200 and 300 mg L^{-1}).

Materials

The hot-rolled deformed steel bars Fe B500B used in this study were provided by Diler Demir Celik Endustri Ve Ticaret A.S. (Gebze, Turkey) has the following composition: 0.20 wt.% C, 0.22 wt.% Si, 0.023 wt.% S, 0.014 wt.% P, 0.84 wt.% Mn, 0.11 wt.% Ni, 0.10 wt.% Cr, 0.017 wt.% Mo, 0.30 wt.% Cu, 0.0012 wt.% V, 0.0095 wt.% N, 0.0002 wt.% B and balance Fe.

Weight loss measurement

For weight loss measurements, Fe B500B samples were cut into cylinders of 5 cm in length and 0.8 cm in diameter. They were ground with different emery papers (*i.e.*, 180, 240, 320, 500, and 1000 grit), washed with bi-distilled water, and degreased with acetone in an ultrasonic bath for 5 minutes. The samples were measured and marked before weighing with an accuracy of 0.0001 g and then immersed in the 0.5 M H$_2$SO$_4$/0.5 M HCl solution without and with the walnut fruit septum extract at 298 K. Before immersing the samples, the solutions were deaerated for 30 min. The kinetics of the corrosion process for the optimum concentration of walnut fruit septum extract was also investigated within the 298 to 318 K temperature range. A water bath was used to keep the temperature constant (±0.5 °C). Adsorption isotherms were also used to find the type of adsorption of the inhibitor on the surface of Fe B500B samples.

After 100 h of immersion, the samples were washed with bi-distilled water, cleaned from corrosion products with 1 M HCl containing 2 g L^{-1} urotropine solution, degreased with acetone, and weighed accurately. Experiments were carried out in triplicates. The corrosion rate (C.R., g m^{-2} h^{-1}) was calculated by Equation (1):

C.R. = *W* / *St*   (1)

where *W* is the average weight loss of the samples in g, *S* is the total surface of the samples in m^2, and *t* is the immersion time in hours.

The corrosion rate (CR, mm year^{-1}) was calculated using converting Equation (2):

CR = (8.76 / d_{Fe}) C.R.   (2)

where *d* is the density of Fe / g cm^{-3} and 8.76 is the conversion coefficient.

The corrosion inhibition efficiency (IE, %) and degree of surface coverage (θ) of the walnut fruit septum extract were calculated by Equations (3) and (4):

$$IE = \frac{C.R.^{\circ} - C.R.}{C.R.^{\circ}} 100 \tag{3}$$

$$\theta = \frac{C.R.^{0} - C.R.}{C.R.^{0}} \tag{4}$$

where C.R. and C.R.^{0} represent the corrosion rates with and without the walnut fruit septum extract, respectively.

Electrochemical methods

Open circuit potential (OCP), potentiodynamic polarization (PD), and electrochemical impedance spectroscopy (EIS) experiments were carried out with IS-CCS Corrosion Cell Set from PalmSens, consisting of a three-electrode cell with a platinum counter electrode (CE) and saturated calomel electrode (SCE) coupled to a Luggin capillary as a reference electrode. The working electrode samples

were coupons with a surface area of 0.785 cm^2. The coupons were cut from hot-rolled deformed steel bars (Fe B500B) in discs of 5 mm in height and 15 mm in diameter that were ground with different emery papers (*i.e.,* 180, 240, 320, 500, and 1000 grit), washed with bi-distilled water and degreased with acetone. Potentiodynamic polarization and electrochemical impedance spectroscopy measurements were carried out using Palmsens 4 potentiostat. The open circuit potential (OCP) of the Fe B500B samples immersed in the mixed acidic medium (0.5 M H$_2$SO$_4$/ 0.5 M HCl) solution was measured for 30 min, with and without additions of the walnut fruit septum extract. Potentiodynamic polarization curves were obtained with a scan rate of 0.1 mV s^{-1} in the potential range OCP ±120 mV. Electrochemical impedance spectroscopy (EIS) was carried out at OCP condition with an amplitude of 10 mV and a frequency range from 1 MHz to 0.01 Hz. The effect of the concentration of the walnut fruit septum extract on the corrosion susceptibility of the Fe B500B samples was tested at 298 K. Meanwhile, the impact of temperature on the corrosion rate and charge transfer resistance of the Fe B500B samples immersed in the mixed acidic medium (0.5 M H$_2$SO$_4$/0.5 M HCl) containing the optimum concentration of walnut fruit septum extract was also tested at 308 and 318 K.

From potentiodynamic results, corrosion rates (CR, mm y^{-1}) were calculated using Equation (5):

$$CR = \frac{Kai}{nd} \tag{5}$$

where *K* is the conversion coefficient (0.00327), *a* is the atomic mass of Fe (g mol^{-1}), *i* is corrosion current density in μA cm^{-2}, *d* is the density of Fe (g cm^{-3}), and *n* is the valence of Fe (*n*=2).

The corrosion inhibition efficiency (IE) of the walnut fruit septum extract was calculated by Equation (6):

$$IE = \frac{i^0_{corr} - i_{corr}}{i^0_{corr}} 100 \tag{6}$$

where *i*$_{corr}$ and *i*$^0_{corr}$ represent the corrosion current density of the samples in the mixed acidic medium (0.5 M H$_2$SO$_4$/0.5 M HCl) with and without the addition of the walnut fruit septum extract, respectively.

Surface characterization of Fe B500B steel bars

The scanning electron microscope (SEM) experiments were conducted using Zeiss EVO MA10. Samples were immersed for 24 h in a blank and 300 mg L^{-1} extract solution of the inhibitor over a temperature range (298 to 318 K). To characterize the surface of Fe B500B samples in the 400 to 4000 cm^{-1} range, attenuated total reflection Fourier transform infrared (ATR-FTIR) spectroscopy with an ALPHA II spectrometer from Bruker was used.

UV-vis spectroscopy analysis

UV-Vis model VWR type UV-1600PC was employed to qualitatively analyze the walnut fruit septum extract's composition. It was performed after 24 h of immersion of Fe B500B samples in the absence and presence of walnut fruit septum extract.

Results and discussion

Weight loss measurements

As shown in Table 1, the corrosion rates (C.R.) of the Fe B500B samples immersed in the mixed acidic medium (0.5 M H$_2$SO$_4$/0.5 M HCl) at 298 K decreased gradually with the increase of the inhibitor concentration. The corrosion rate decreased from 1.4117 to 0.2893 g m^{-2} h^{-1} in terms of weight loss

over time or decreased from 1.5713 to 0.3220 mm y^{-1} in terms of penetration in the Fe B500B samples surface samples over time at 298 K. Inhibitor efficiency and surface coverage increased with increasing the extract concentration, reaching a maximum value of 79.51 % for 300 mg L^{-1} of walnut fruit septum extract added. Further increase of inhibitor concentration (*i.e.,* 400 mg L^{-1}, results are not displayed) does not improve the inhibitor efficiency, suggesting that 300 mg L^{-1} is the optimum concentration. This will be further confirmed by SEM analysis. The addition of the inhibitor changes the type of corrosion to the uniform type.

Table 1. *Weight loss results of Fe B500B samples immersed for 100 h at 298 K in the mixed acidic medium (0.5 M H$_2$SO$_4$/0.5 M HCl) without and with different concentrations of walnut fruit septum extract*

Concentration, mg L^{-1}	C.R., g m^{-2} h^{-1}	CR, mm y^{-1}	IE, %
0.0 (blank)	1.4117	1.5713	-
100.0	0.7966	0.8866	43.58
200.0	0.4831	0.5377	65.78
300.0	0.2893	0.3220	79.51

Adsorption isotherm

It is generally known that inhibitor molecules adsorb on the metal surface by chemisorption (involving coordination bonds or covalent bonds between inhibitor molecules and unfilled d orbitals of iron) in the case of Fe B500B samples, or physical adsorption on the surface of the metal (involving electrostatic forces). Therefore, adsorption isotherms are used to gain information on the type of interaction on the surface of the metal. Various isotherms, such as Temkin, Freundlich, Langmuir, Frumkin, El-Awady, and Flory-Huggins, were used to fit the data reported in Table 1. Nonetheless, the best-obtained fit was Flory-Huggins adsorption isotherm, as shown in Figure 1. The data for adsorption isotherms were fitted according to Equation (7):

$$\ln\left(\frac{\theta}{C_{inh}}\right) = \ln K_{ads} + x \ln(1-\theta) \tag{7}$$

where θ is the surface coverage assessed from weight loss measurement at 298 K (Table 1). The intercept and the slope from the plot presented in Figure 1 are ln K_{ads} and x, respectively, where K_{ads} is the adsorption equilibrium constant, and x represents the number of water molecules substituted by a single inhibitor molecule [24]. The intercept value of the Flory-Huggins isotherm presented in Figure 1, which corresponds to ln K_{ads} was found to be 1.78 and is further used to calculate the standard Gibbs free energy of the adsorption according to Equation (8):

$$\Delta G°_{ads} = - RT \ln (55.5 \Delta K_{ads}) \tag{8}$$

where R is the universal gas constant in 8.314 J mol^{-1} K^{-1}, T is the temperature in Kelvin, 55.5 mol L^{-1} is the concentration of water in solution at 298 K. Based on the literature [25], if the value of Gibbs free energy of the adsorption ($\Delta G°_{ads}$) is less negative or equal to -20 kJ mol^{-1}, the interaction between the charged metal surface and the inhibitor molecules is by physical adsorption (electrostatic). In the case when $\Delta G°_{ads} \geq$ -40 kJ mol^{-1}, we have the occurrence of chemisorption (charge transfer between the inhibitor molecules and metal surface) [25]. The calculated value in this case is -14.38 kJ mol^{-1}, confirming physisorption. The x value is 0.49, which indicates the replacement of water molecules.
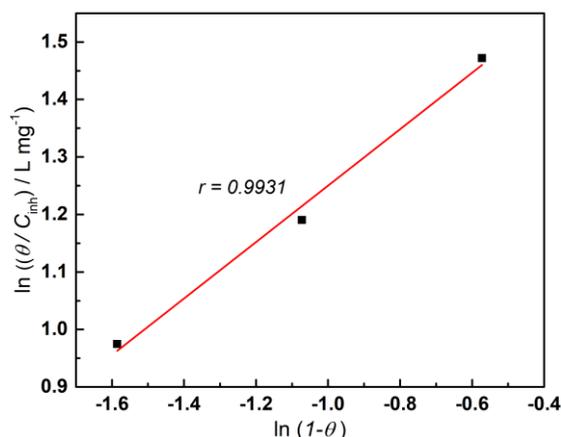
Figure 1. *Adsorption isotherm of Flory-Huggins plotted from the weight loss measurements data at 298 K*

Effect of temperature and thermodynamic activation parameter

Temperature has a significant effect on the kinetics of the corrosion processes. It also impacts the behaviour of the corrosion inhibitors. To study these effects, weight loss measurements at different temperatures (298 to 318 K) with and without the addition of the optimum concentration of the walnut fruit septum extract (300 mg L^{-1}) were performed. As shown in Table 2, the corrosion rate increases significantly with the increase of the temperature for blank and inhibited solutions that corresponds to the Arrhenius equation (9).

Table 2. *Corrosion rate of Fe B500B samples and inhibitor efficiency of walnut fruit septum extract for optimum concentration and blank after 100 h immersion at 298 to 318 K*

C / mg L^{-1}	Temperature, K					
	298		308		318	
	C.R., g m^{-2} h	IE, %	C.R., g m^{-2} h	IE, %	C.R., g m^{-2} h	IE, %
0.0 (blank)	1.4117	-	6.5271	-	18.2326	-
300.0	0.2893	79.51	2.5262	61.29	8.3767	54.05

To further investigate this process, the Arrhenius-type dependence between temperature and corrosion rate was used, from which we were able to calculate the activation energy of the corrosion process (E_a) at different temperatures for the blank and optimum concentration of the inhibitor, using Equation (9) [26]:

$$\text{C.R.} = k \, e^{\left(\frac{-E_a}{RT}\right)} \tag{9}$$

By using the transition state energy equation (10), thermodynamic parameters for the corrosion processes, such as entropy (ΔS_a) and enthalpy (ΔH_a) were calculated [26]:

$$\text{C.R.} = \frac{RT}{Nh} e^{\left(\frac{\Delta S_a}{RT}\right)} e^{\left(\frac{-\Delta H_a}{RT}\right)} \tag{10}$$

where C.R., k, N, and h are the corrosion rate, pre-exponential factor, Avogadro number and Planck's constant, respectively.

From the slope in Figure 2a, which is according to the linearized form of Equation (9), equal to -E_a/R, the activation energy of the metal dissolution was calculated for the blank and optimum concentration of the inhibitor (300 mg L^{-1}). Figure 2b shows the plot of ln [C.R. T^{-1}) *vs.* T^{-1} from which the intercept and slope were found and used to calculate (ΔS_a) and (ΔH_a) values, respectively.
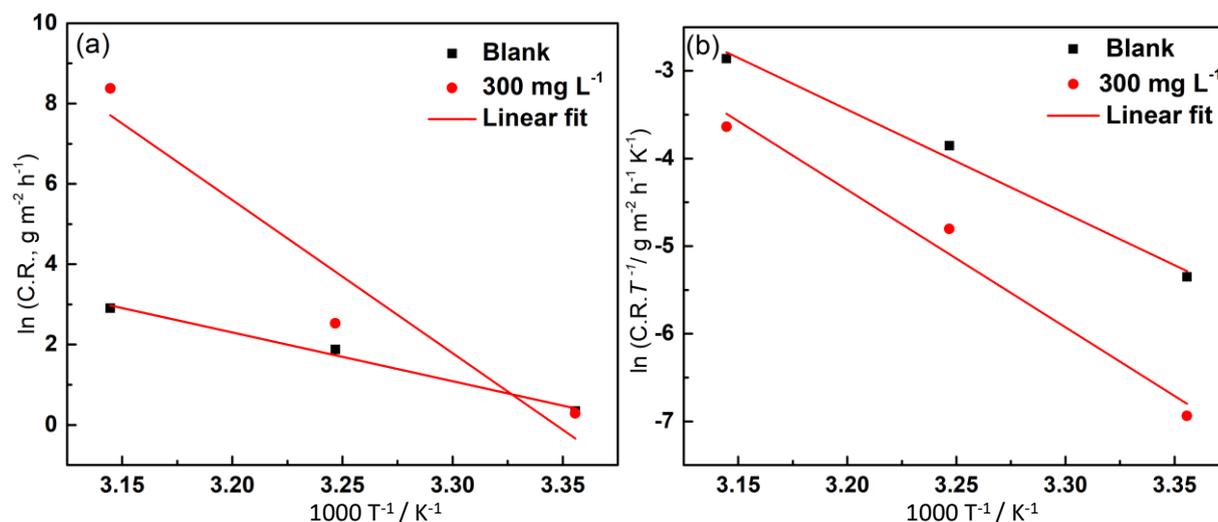
Figure 2. *(a) Plot of ln C.R. vs. 1/T for the activation energy of corrosion reaction, (b) Arrhenius plot of ln (C.R./T) vs. 1/T for Fe B500B samples in the absence and presence of optimum concentration (300 mg L^{-1}) of walnut fruit septum extract*

Table 3 shows the activation parameters obtained from Arrhenius and transition state plots. From the calculated data listed in Table 3, the activation energy for the inhibitor optimum concentration was higher than the blank solution. The activation energy for optimum concentration (300 mg L^{-1}) and blank solution were 316.92 and 100.93 kJ mol^{-1}, respectively. This indicates that walnut fruit septum extract forms a thin protection layer for corrosion mitigation in the inhibited medium [27]. This increase in the E_a value suggests a physisorption that occurs at the first stage of the inhibition mechanism [28]. The enthalpy of activation (ΔH_a) has a positive sign, which implies an endothermic corrosion process in the Fe B500B samples. Interestingly, both activation energy E_a values for the blank and optimum inhibitor concentration are greater than the corresponding ΔH_a values. This indicates the involvement of a gaseous reaction in the corrosion process, that is, the reduction of the hydrogen ions [29]. The positive value of entropy shows an increase in the disorder.

Table 3. *The values of E$_a$, ΔH$_a$, and ΔS$_a$ for Fe B500B samples immersed for 100 h in the mixed acidic medium (0.5 M H$_2$SO$_4$/0.5 M HCl) in the absence and the presence of 300 mg L^{-1} of walnut fruit septum extract*

C / mg L^{-1}	E_a / kJ mol^{-1})	ΔH_a / kJ mol^{-1}	ΔS_a / J mol^{-1} K^{-1}
0.0 blank	100.93	98.35	286.08
300.0	316.92	130.19	379.86

Potentiodynamic polarization curves

Figure 3 shows the potentiodynamic polarization curves for Fe B500B samples in the mixed acidic medium (0.5 M H$_2$SO$_4$/0.5M HCl) at 298 K without and with different concentrations of the walnut fruit septum extract. The addition of the walnut fruit septum extract lowers both cathodic and anodic branches of the potentiodynamic polarization curves, with more dominance on the anodic side. All cathodic and anodic branches are parallel, suggesting that the inhibition mechanism has not been changed [30].

Table 4 presents the Tafel extrapolation data, including corrosion potential (E_{corr}), corrosion current density (i_{corr}), polarization resistance (R_p) and the respective calculated corrosion rates and inhibitor efficiencies.
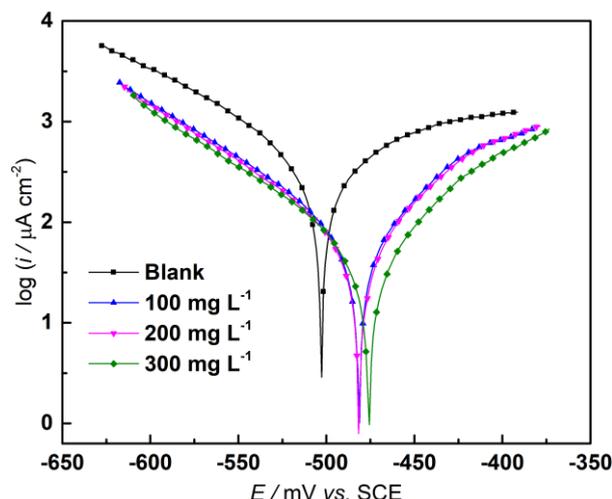
Figure 3. *Potentiodynamic polarization curves of Fe B500B samples in the mixed acidic medium (0.5 M H₂SO₄/0.5 M HCl) solution without and with different concentrations of the walnut fruit septum extract at 298 K*

Table 4. *Kinetic parameters obtained from potentiodynamic polarization curves of Fe B500B samples immersed in the mixed acidic medium (0.5 M H₂SO₄/ 0.5 M HCl) at 298 K, without and with different concentrations of walnut fruit septum extract*

C / mg L^{-1}	E_{corr}/ mV	b_c / mV dec^{-1}	b_a / mV dec^{-1}	i_{corr} / μAcm^{-2}	CR, mm year^{-1}	IE, %	f_a	f_c	R_p / Ω cm^2	IE$_{Rp}$ / %
0	-504.79	-84.65	138.8	316.04	3.695	-			72.24	-
100	-475.68	-89.719	60.688	65.660	0.714	80.68	0.13	0.15	239.40	69.82
200	-476.98	-80.8	55.516	51.222	0.596	83.88	0.09	0.11	278.95	74.10
300	-466.79	-88.012	49.528	41.324	0.481	86.99	0.06	0.085	333.01	78.31

As shown in Table 4, E_{corr} value shifts positively compared to the blank solution. Based on the literature, when the difference in corrosion potential between the inhibited solution and blank is less than 85 mV in absolute value, this inhibitor is considered a mixed-type inhibitor with anodic dominance [31]. Cathodic (b_c) and anodic (b_a) Tafel slopes decrease in their absolute values, indicating adsorption of the inhibitor on both cathodic and anodic sites [32]. Current density (i_{corr}) values decrease significantly with the increase of walnut fruit septum extract concentration from 316.04 μA cm^{-2} for the blank solution to 41.32 μA cm^{-2} for the optimum inhibitor concentration of 300 mg L^{-1}. Corrosion rates also decrease from 3.695 mm year^{-1} for blank solution to 0.481 mm year^{-1} for the optimum concentration. These results are in general agreement with corrosion rates obtained from weight loss results (Table 1), except for the blank solution, what is probably due to pitting corrosion occurring in this aggressive condition. In such a case, CR cannot be estimated by the weight loss method. The repeatability of the results regarding the corrosion rate refers to the uniform corrosion, not the pitting corrosion. Increasing the exposure time and temperature in weight loss measurements, as well as adding the inhibitor, converts pitting corrosion to uniform corrosion.

Regarding penetration measurements, the corrosion rate decreased from 3.69 mm year^{-1} for the blank solution to 0.48 mm year^{-1} for the optimum concentration (300 mg L^{-1}). The inhibitor efficiency increases remarkably with the increase of the inhibitor concentration, reaching a maximum value for optimum concentration (300 mg L^{-1}) of 86.99 %. Further increase of inhibitor concentration (*i.e.*, 400 mg L^{-1} results not displayed) did not result in increased inhibition efficiency.

To clarify the complexity of the corrosion process that occurred at the metal/solution interface in the presence of the inhibitor (supposed electrochemical inhibition mechanism), Cao [33]

suggested two exponents of the cathodic (f_c) and anodic (f_a) reaction, calculated by equations (11) and (12):

$$f_c = \left(\frac{i_{corr}^{inh}}{i_{corr}^0} \right) e^{\frac{E_{corr}^{inh} - E_{corr}^0}{b_c}} \tag{11}$$

$$f_a = \left(\frac{i_{corr}^{inh}}{i_{corr}^0} \right) e^{\frac{E_{corr}^0 - E_{corr}^{inh}}{b_a}} \tag{12}$$

where the super-indexes (0) and (inh) represent the corrosive medium without and with walnut fruit septum extract, respectively. The inhibitive mechanism is attributed to the geometric blocking effect if $f_c = f_a$, and if $f_c < 1$ or $f_a < 1$, the blocking effect of active sites is attributed to the adsorption of the inhibitor.

The calculated values of f_a and f_c are also displayed in Table 4. Both coefficients, f_c and f_a, are less than one, and furthermore, $f_c > f_a$. This indicates that the inhibition process is related to the adsorption on the active sites of the metal surface. Meanwhile, the inhibitor retards the anodic reaction. This confirms the shift of E_{corr}, shown in Figure 3 and Table 4.

In addition, the Stearn-Geary equation was used to calculate the polarization resistance (R_p) by equation (13):

$$R_p = \frac{b_c b_a}{2.303\, i_{corr} \left(b_c + b_a \right)} \tag{13}$$

Inhibitor efficiency for R_p values was calculated by equation (14):

$$IE_{R_p} = \frac{R_{p\ inh} - R_{p\ 0}}{R_{p\ inh}} 100 \tag{14}$$

where $R_{p\ inh}$ is polarization resistance with the presence of the inhibitor, and $R_{p\ 0}$ is the polarization resistance of the blank solution.

Table 4 shows that R_p values increase with the increase of walnut fruit septum extract concentration from 72.24 Ω cm^2 for the blank solution to 333.0 Ω cm^2 for optimum concentration (300 mg L^{-1}). The increase in concentration of the inhibitor corresponds to the increase in polarization resistance. This indicates the reduction of the electroactive area by the adsorption film formed by the inhibitor on the surface of Fe B500B steel bar samples.

Effect of temperature on the corrosion rate of Fe B500B samples

Potentiodynamic polarization was also used to investigate the effect of temperature on corrosion rate. Figure 4 presents polarization curves for Fe B500B samples in the mixed acidic medium (0.5 M H$_2$SO$_4$/0.5 M HCl) for blank and optimum concentration (300 mg L^{-1}) at different temperatures. Both anodic and cathodic branches of polarization curves followed the same trend with the increase in temperature. It is clearly seen that with the addition of the optimum concentration of the inhibitor, the corrosion current density significantly decreases compared to the corresponding blank solutions at all tested temperatures.

All relevant data evaluated from potentiodynamic polarization curves are summarized in Table 5, where it is seen that corrosion current density values decrease with the increase of temperature, and this is also reflected in the variation of the inhibition efficiency values. The shift of corrosion potential toward the anodic side decreases with the increase in temperature. At 318 K, the corrosion potential shifts slightly to the cathodic side, referred to the corresponding blank solution (Figure 4).
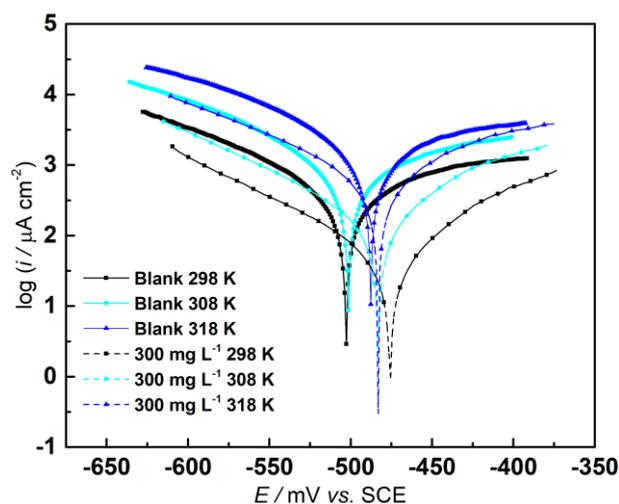
Figure 4. *Potentiodynamic polarization curves of Fe B500B samples in the mixed acidic medium (0.5 M H$_2$SO$_4$/0.5 M HCl) without and with the optimum concentration (300 mg L^{-1}) of the walnut fruit septum extract at different temperatures (298 to 318 K)*

This confirms that walnut fruit septum extract acts as a mixed-type inhibitor with dominance on the anodic side, which decreases with the increase in temperature. As a consequence of the increase in temperatures, the density of the pits (active centres of adsorption) increases until the formation of uniform corrosion [25]. This justifies again the mechanism of inhibition of walnut fruit septum alcoholic extract suggested by weight loss to convert pitting corrosion into uniform corrosion [34].

Table 5. *Data obtained from Tafel extrapolation of potentiodynamic polarization curves for Fe B500B samples immersed in the mixed acidic medium (0.5 M H$_2$SO$_4$/ 0.5 M HCl) without and with the optimal concentration of 300 mg L^{-1} walnut fruit septum extract at different temperatures (298-318 K)*

| C / mg L^{-1}	E$_{corr}$ / mV	b$_c$ / mV dec^{-1}	b$_a$ / mV dec^{-1}	i$_{corr}$ / μA cm^{-2}	CR, mm year^{-1}	IE, %	R$_p$ / Ω cm^2	IE$_{R_p}$%
0.0 (blank) 298 K	-504.79	- 84.65	138.8	316.04	3.695	-	72.24	-
0.0 (blank) 308 K	- 483.34	- 95.85	205.41	851.14	9.87	-	33.34	-
0.0 (blank) 318 K	- 487.69	- 109.90	280.44	1854.90	21.52	-	18.48	-
300.0 298 K	- 466.79	- 88.012	49.528	41.324	0.481	86.99	333.02	78.31
300.0 308 K	- 496.17	- 90.79	115.73	217.82	2.53	74.4	101.42	67.1
300.0 318 K	- 485.28	- 100.66	113.52	608.84	7.06	67.2	38.05	51.4

To investigate further, the Stearn-Geary equation (equation 13) was also used here to calculate polarization resistance. Since polarization resistance is the inverse of current density, its decrease means an increase in current density or, in other words, an increase in the corrosion rate. Inhibitor efficiency calculated from R$_p$ values decreases with the increase in temperature. This indicates a decrease in the performance of the inhibitor at high temperatures.

Electrochemical impedance spectroscopy measurements

Electrochemical impedance spectroscopy was conducted for Fe B500B samples immersed in the mixed acidic medium (0.5 M H$_2$SO$_4$/0.5 M HCl) without and with different concentrations of the

A. Lame *et al.*

J. Electrochem. Sci. Eng. **14(3) (**2024) 297-320

inhibitor at 298 K, and also at 308 and 318 K for the optimum inhibitor concentration (300 mg L^{-1}) with respective to blank solution.

Figure 5a shows the Nyquist diagrams of Fe B500B samples in the presence and absence of the walnut fruit septum at 298 K. The obtained semicircle impedance responses indicate that the process occurring at the metal interface with the solution is mainly charge transfer [35]. Furthermore, all semicircles appear slightly depressed. This may be related to the inhomogeneous surface of Fe B500B samples that causes frequency dispersion of the interfacial impedance [36]. At lower frequencies, an inductive loop that may be related to the adsorption-desorption of the inhibitor molecules due to electrode surface instability is observed. Nevertheless, this inductive loop decreases with the increase of the inhibitor concentration, indicating the increase of stability in the adsorption-desorption equilibrium process at the electrode surface [36]. The Nyquist plots display a significant increase in diameters with the addition of the walnut fruit septum extract. This indicates an increase in the adsorption of the inhibitor with the increase of the concentration, resulting in a lower electroactive region on the surface of the Fe B500B samples. Bode modulus and phase angle diagrams for Fe B500B samples immersed in the mixed acidic medium (0.5 M H$_2$SO$_4$/0.5 M HCl) without and with different concentrations of the inhibitor at 298 K are displayed in Figure 5b. As shown in Bode curves at lower frequencies, the impedance magnitude increases with the concentration of walnut fruit septum extract. This reveals higher charge transfer resistance at the metal solution interface. It seems that the corrosion mechanism does not change with the increase of the inhibitor concentration, which is shown by forms of Bode curves that are similar in shape for all measured samples. Only one peak appearing in phase angle plots indicates the presence of only one time constant. With the increase of the inhibitor concentration, the phase angle peak increases, which suggests continuous adsorption of inhibitor molecules on the Fe B500B samples at higher concentrations of the inhibitor. The increase in phase angle value with the increase of inhibitor concentration indicates that the metal dissolution decreased [37].
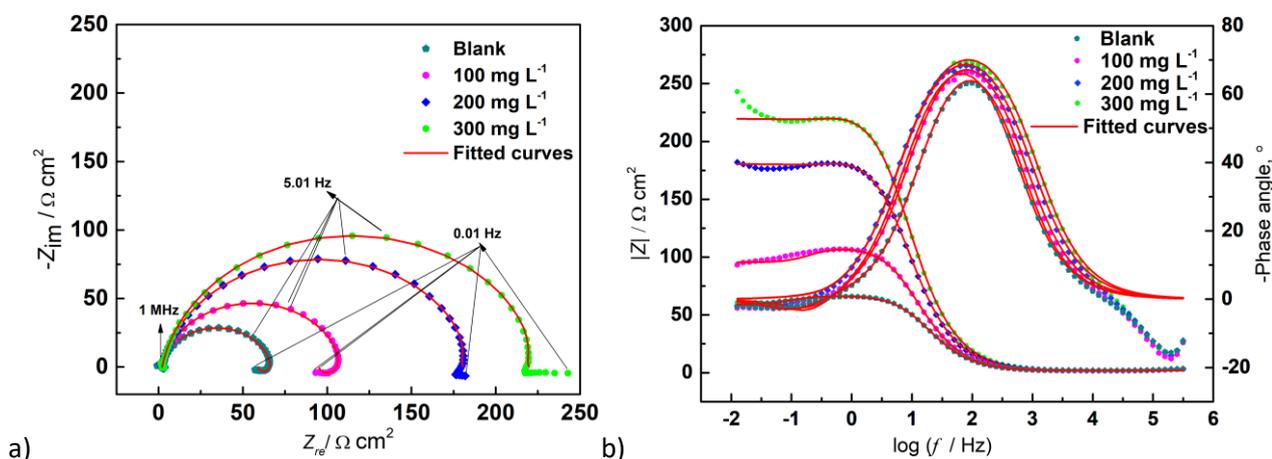
Figure 5. *(a) Nyquist plots and (b) Bode phase angle and modulus plots for Fe B500B samples in the mixed acidic medium (0.5 M H$_2$SO$_4$/0.5 M HCl) without and with different concentrations of the walnut fruit septum extract at 298 K*

Figure 6 shows Nyquist and Bode diagrams at different temperatures for the optimum concentration of the walnut fruit septum extract (300 mg L^{-1}) and blank solution. The capacitive loops increase for optimum concentration compared to respective blank solutions at all studied temperatures, indicating the formation of the protective layer on the surface of Fe B500B samples. Nevertheless, the capacitive loops decrease with the increase of the temperature both for blank and

optimum concentration, implying acceleration of corrosion rate. The respective Bode modulus plots show an increase in the magnitude of impedance for optimum concentration (300 mg L^{-1}) compared with corresponding blank solutions. However, the increase in temperature decreases the magnitude of the impedance, indicating the desorption of inhibitor molecules with the increased temperature.
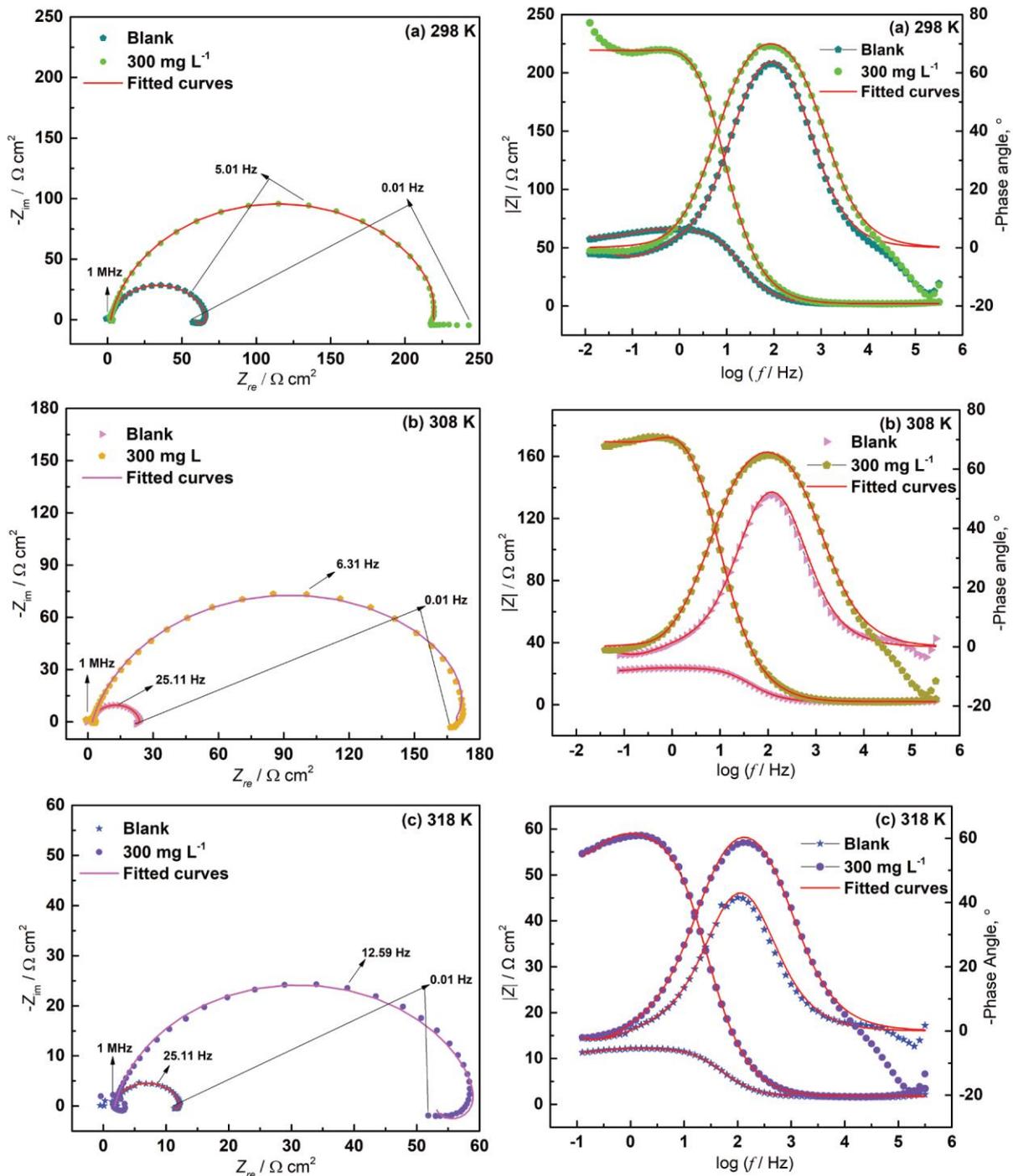
Figure 6. *Nyquist plots (left), and Bode phase and-modulus plots (right) for Fe B500B samples in the mixed acidic medium (0.5 M H$_2$SO$_4$/0.5 M HCl) without and with the optimum concentration (300 mg L^{-1}) of the walnut fruit septum extract at: (a) 298 K; (b) 308 K; (c) 318 K*

The equivalent circuit shown in Figure 7 was used to fit the data of EIS measurements. Experimental data obtained from Palmsens 4 potentiostat were imported to Aftermath software version 1.6.10523 from Pine Research to make fittings of EIS spectra.
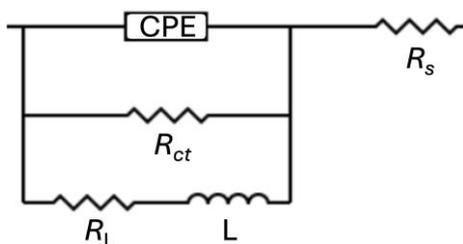
Figure 7. Equivalent circuit used to fit the EIS experimental data

The solution resistance (R_s), constant phase element (CPE), which is related to double layer capacitance, charge transfer resistance (R_{ct}), inductance (L), and resistance of inductance (R_L) were used to fit the experimental data of EIS measurements. Equation (15) determines the impedance of constant phase element (Z_{CPE}) [38]:

$$Z_{CPE} = \frac{1}{Y_0 (j\omega)^{\alpha}} \qquad (15)$$

where Y_0 represents the CPE constant, ω ($\omega = 2\pi f$) is the angular frequency, and α is the CPE exponent, which represents a deviation from the ideal semicircle response and takes value in a range of $-1 < \alpha < 1$. When α is equal to 1, 0 and -1 represent a pure capacitor, resistor, and inductor, respectively. The CPE was further converted to double-layer capacitance (C_{dl}) by equations (16) and (17):

$$C_{dl} = Y_0 \, \omega_{max}^{\alpha-1} \qquad (16)$$

$$\omega_{max} = 2\pi f_{max} \qquad (17)$$

where f_{max} is the frequency for the maximum value of the imaginary component in the plot of $-Z_{im}$ *vs.* $\log f$ (12.62, 7.95, 6.30, and 6.31 Hz for the walnut fruit septum extract concentration of 0 (blank), 100, 200 and 300 mg L^{-1} respectively), whereas ω_{max} is the maximum angular frequency calculated from f_{max}.

The results of the equivalent circuit fitting to experimental impedance data presented in Figures 5 and 6 are shown in Tables 6 and 7.

Table 6 presents impedance parameter values for Fe B500B samples in a blank solution and for different concentrations of the walnut fruit septum extract at 298 K.

Table 6. Fitted experimental parameter values of EIS spectra (Fig.5) for Fe B500B samples immersed in the mixed acidic medium (0.5 M H_2SO_4/0.5 M HCl), without and with different concentrations of walnut fruit septum extract at 298 K

C / mg L^{-1}	R_s / Ω cm^2	R_{ct} / Ω cm^2	C_{dl} / μF cm^{-2}	α	L / H cm^2	R_L / Ω cm^2	IE, %
0.0 (blank)	1.99	64.82	185.66	0.92	772.01	478.81	-
100.0	2.33	111.17	164.47	0.91	1044.05	860.50	41.69
200.0	2.11	186.33	135.64	0.89	1338.08	4212.50	65.21
300.0	2.10	225.94	111.91	0.90	1953.93	5863.68	71.31

It is shown in Table 6 that the addition of walnut fruit septum extract increases the value of charge transfer (R_{ct}), indicating the adsorption of the inhibitor molecules at the metal-solution interface with the increase of the inhibitor concentration. As a consequence, the corrosion rate is decreased. The double-layer capacitance (C_{dl}) decreases as the corrosion inhibitor concentration increases. The behaviour of the double-layer capacitance can be investigated further by using the following equation [39]:

$$C_{dl} = \frac{\varepsilon^0 \varepsilon}{d} S \tag{18}$$

where ε^0 and ε are vacuum dielectric permittivity constant and double layer dielectric constant, respectively. *S* is the exposed area of material in the corrosive medium, and *d* is the thickness of the double layer. The dielectric constant of water is bigger than that of inhibitor molecules. The decrease of the double-layer capacitance values suggests a continuous replacement of water molecules at the metal solution interface by adsorption of the inhibitor molecules with the increase of the inhibitor concentration. The molecules of the inhibitor are bigger than the molecules of water, indicating an increase in *d*, which results in a decrease of capacitance [40]. The inductance values increase with the increase of the inhibitor concentration to resist the current changes. This is further supported by the corresponding values of R_L, which also increase with the increase of the inductance values. This phenomenon may result from either the surface of the metal becoming less tense or from the formation of unstable corrosion products, such as $FeCl_2$, at the boundary between the metal and the solution, causing the inductive loop (*R L*) at low frequencies [41].

Table 7 lists impedance parameter values for Fe B500B samples measured in blank solution and for the optimal concentration of the walnut fruit septum extract (300 mg L^{-1}) at different temperatures (298 to 318 K). The parameter values were obtained by fitting EEC in Figure 7 to impedance spectra presented in Figure 6. As shown in Table 7, the charge transfer resistance (R_{ct}) increases at the optimum inhibitor concentration compared to the respective blank solution, displaying the moderate performance of the inhibitor at higher temperatures. The increase in the temperature decreases charge transfer resistance both for blank and optimum concentration. This suggests increased desorption of the inhibitor molecules from the metal solution interface. Double-layer capacitance (C_{dl}) value decreases compared to the blank solution and increases with the increase of the temperature. The values of inductance (*L*) decrease with the increase in temperature, indicating increased current at the metal/solution interface. Also, resistance R_L follows the same trend as inductance with the increase in temperature.

Table 7. *Fitted experimental parameter values of EIS spectra (Fig.6) for Fe B500B samples immersed in the mixed acidic medium (0.5 M H_2SO_4/0.5 M HCl) without and with 300 mg L^{-1} walnut fruit septum extract at different temperatures (298-318 K)*

Inhibitor concentration, mg L^{-1}	R_s / Ω cm^2	R_{ct} / Ω cm^2	C_{dl} / μF cm^{-2}	α	L / H cm^2	R_L / Ω cm^2
0.0 (blank) - 298 K	1.99	64.82	185.66	0.92	772.01	478.81
0.0 (blank) - 308 K	1.83	22.09	248.98	0.91	182.35	185.86
0.0 (blank) - 318 K	1.68	10.65	396.60	0.90	49.58	84.19
300.0 - 298 K	2.10	225.94	111.91	0.90	1953.93	5863.68
300.0 - 308 K	2.05	182.86	122.79	0.86	526.83	2044.81
300.0 - 318 K	1.83	58.56	151.79	0.88	261.51	411.88

SEM analysis

Scanning electron microscope (SEM) was used to evaluate the protective properties of walnut fruit septum extract on the surface of Fe B500B samples immersed in the mixed acidic medium (0.5 M H_2SO_4/0.5 M HCl), without and with optimum inhibitor concentration (300 mg L^{-1}), in the temperature range 298-318 K.

Figure 8a shows the Fe B500B sample surface previously polished with emery paper and cleaned with bi-distilled water before immersion. From the observation of the image, some white lines appear on the surface of the sample that are inherent from the polishing machine. At 298 K, the SEM image of the sample in the blank solution shows local corrosion (Figure 8b).
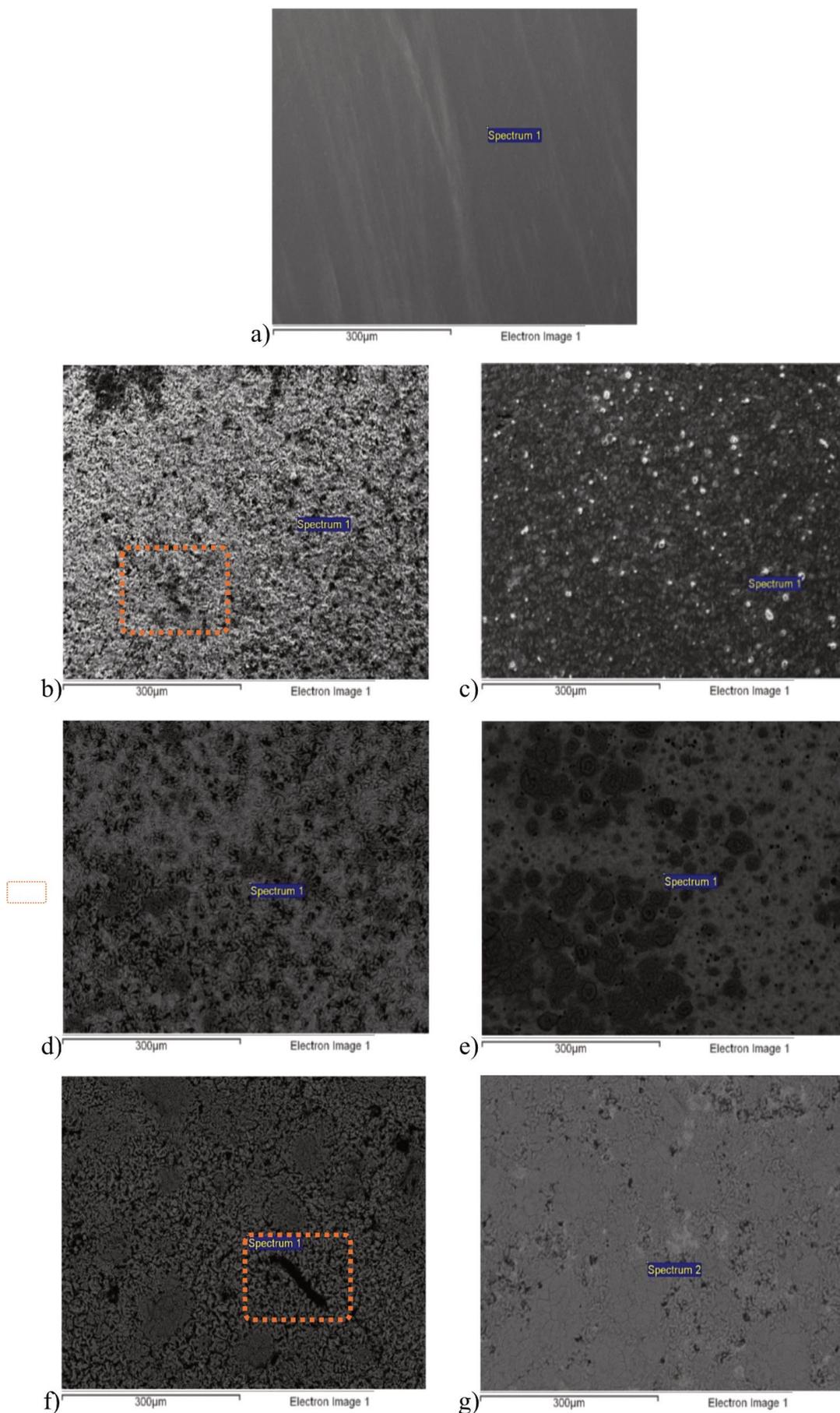
Figure 8. *SEM images of Fe B500B samples: (a) polished, (b, d, f) immersed in blank solution, (c, e, g) in optimum concentration (300 mg L^{-1}) of walnut septum fruit extract, for 24 h at 298, 308 and 318 K*

The sample immersed in the solution with optimum inhibitor concentration at 298 K displays a homogeneous and uniform surface (Figure 8c), conforming the results from weight loss and electro-chemical measurements. The SEM images confirm once more the good protection performance of the inhibitor, as we observe the conversion with time of the localised corrosion to uniform corrosion. This validates the adsorption of the walnut fruit septum extract on the surface of the Fe B500B sample. With the increase in temperature, the protection properties of the walnut fruit septum extract weakened, but the samples immersed in the solution with optimum inhibitor concentration showed improvements compared to the respective samples immersed in blank solutions at the corresponding temperatures (as seen in Figure 8). Namely, the walnut fruit septum extract significantly impedes corrosion processes on the surface of the Fe B500B samples.

ATR-FTIR spectroscopy analysis of the walnut fruit septum extract

Based on previously published works on green inhibitors, the presence of heteroatoms (*i.e.,* O, N and S), aromatic rings, double bonds, and conjugated bonds gave the inhibitors the ability to be adsorbed on the surface of the metals [42,43]. To confirm qualitatively the presence of those groups in walnut fruit septum extract, ATR-FTIR was carried out on Fe B500B samples in polished form, immersed in blank and optimum concentration of the inhibitor and pure alcoholic extract, and shown in Figure 9. The ATR-FTIR of the dried alcoholic extract (Figure 9d) displays the strongest and broader band at 3237 cm^{-1}, which is attributed to O-H stretching [44]. The bands at 2922 and 2852 cm^{-1} are related to C-H stretching vibration [44]. The 1706 cm^{-1} peak is attributed to the carbonyl group, C=O stretching [45]. The strong bands at 1604 and 1518 cm^{-1} could be assigned as aromatic rings supported by weak peaks at 2114 cm^{-1} [44]. The ATR-FTIR spectra for the non-treated specimen (only ground) and the specimen immersed in blank solution show no characteristic bands (Figure 9a and 9b). The FTIR spectrum of the Fe B500B immersed in the optimum concentration of the inhibitor (300 mg L^{-1}) for 24 h displays bands at 1618 and 1018 cm^{-1}, attributed to the stretching vibration of C=C, C=O double bonds and C-O bonds, respectively (Figure 9c).
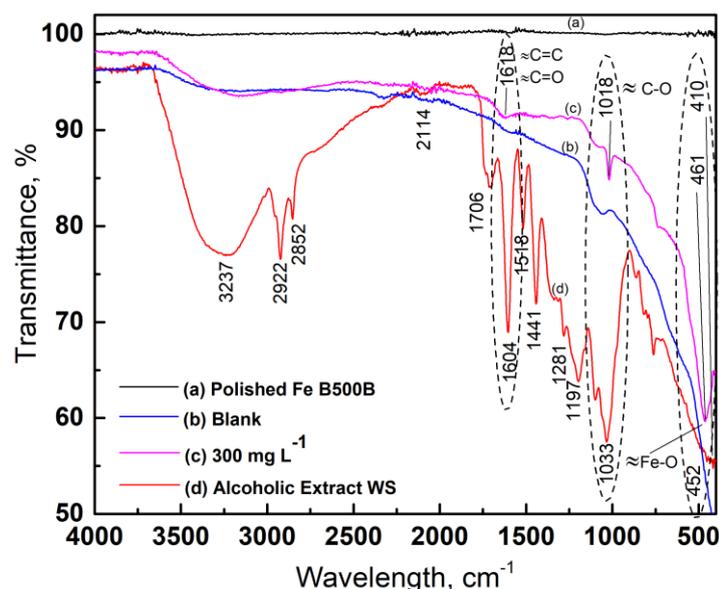
**Figure 9.** *ATR-FTIR spectra of Fe B500B in: (a) polished form, (b) immersed in blank, (c) at optimum inhibitor concentration (300 mg L-1); (d) of pure alcoholic inhibitor extract*

These bands are approximately in the same range as the bands for C=C, C=O, and C-O of phenolic compounds on the alcoholic extract of the walnut septum (Figures 9 c,d) [46,47]. This suggests the presence of phenolic compounds on the surface of the Fe B500B sample. Also, the bands at 461 and

410 cm^{-1} are attributed to the stretching modes of the Fe-O bonds, resulting from the interaction of iron with the oxygen of polyphenols present in the extract [47]. Based on the presence of these bands, it can be concluded that walnut septum extract molecules are chemisorbed on the surface of the Fe B500B specimen.

UV-Vis spectroscopy analysis of the walnut fruit septum extract

Organic compounds in walnut fruit septum extract can reveal characteristic peaks. The alcoholic extract and blank solution (0.5 M H$_2$SO$_4$/0.5 M HCl), with and without the addition of 300 mg L^{-1} (optimum concentration), were used for the analysis. The absorbance peaks are displayed in Figure 10. The immersion of Fe B500B steel bar in the solution that contains the optimum concentration of the inhibitor (300 mg L^{-1}) decreases the absorbance peak compared to the optimum (300 mg L^{-1}) solution without immersion of the Fe B500B samples. This clearly indicates the adsorption of the inhibitor molecules on the active sites on the surface of Fe B500B samples [48].
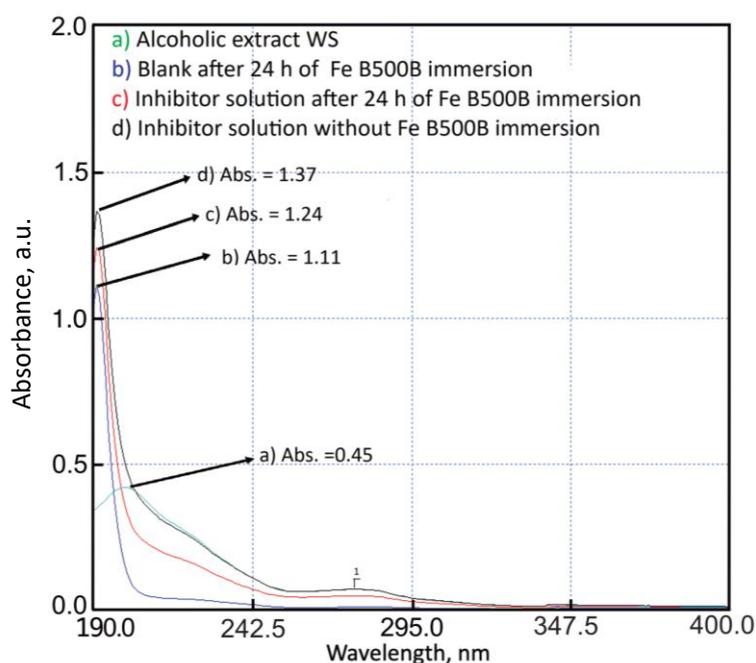
Figure 10. *UV-vis spectra of: (a) alcoholic walnut fruit septum extract; solutions after 24 h immersion of Fe B500B in (b) blank, and (c) inhibitor (300 mg L^{-1}); (d) inhibitor solution without immersion of Fe B500B*

Suggested mechanism of corrosion and inhibition by walnut fruit septum extract

According to the above discussion based on weight loss and electrochemical measurements, walnut fruit septum extract acts as a mixed-type inhibitor (anodic-cathodic) that is adsorbed spontaneously on the surface of the metal (hot rolled steel Fe B500B samples), according to the mixed physical-chemical mechanism. It is well known that carbon steel has a positive surface charge in an acidic solution [49]. According to the potential of the zero-charge adsorption mechanism, for Fe B500B samples, pH of zero charge (pH$_{zch}$) is almost 8.8. When immersed in acidic solutions (pH <8.8), the Fe B500B sample is charged positively. In such conditions, Cl$^-$ ions and other negative ions are likely to get adsorbed. Another important principle proposed by Pearson HSAB (Hard and Soft Acids and Bases) explains the adsorption of Cl$^-$ (as a weak base) and bulk metals, which act as a weak acid [50,51].
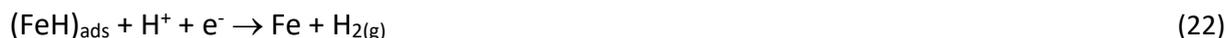
The proposed mechanism for anodic and cathodic corrosion reaction on the surface of carbon steel (hot rolled steel Fe B500B samples) immersed in mixed acidic solution (0.5 M H$_2$SO$_4$/0.5 M HCl) contains the following steps [52-54]:

In water solution, H_2SO_4 and HCl dissociate to H^+, HSO^{4-}, SO_4^{2-} and Cl^- ions. Corrosion of hot-rolled steel Fe B500B in mixed acidic solution is considered as localized corrosion in the form of pitting with hydrogen evolution at the cathodic sites and anodic dissolution of Fe, where HSO_4^-, SO_4^{2-} and Cl^- ions react and form corrosion products as $FeCl_2$, $FeSO_4$, and $Fe(HSO_4)_2$. The presence of Cl^- in concentration 0.5 M with autocatalytic action, the small radius, and easy penetration in the passivation layer accelerates the pitting corrosion, where the presence of SO_4^{2-} ions can act as a pitting corrosion accelerator [53].

The general cathodic reaction is (Equation (19)):

$$2H^+_{(aq)} + 2e^- \rightarrow H_{2(g)} \tag{19}$$

This reaction can be described by the following steps (Equations (20) to (22)):

$$Fe + H^+ \rightarrow (FeH^+)_{aq} \tag{20}$$

$$(FeH^+)_{aq} + e^- \rightarrow (FeH)_{ads} \tag{21}$$

$$(FeH)_{ads} + H^+ + e^- \rightarrow Fe + H_{2(g)} \tag{22}$$

The general anodic reaction is (Equation (23)):

$$Fe \rightarrow Fe^{2+} + 2e^- \tag{23}$$

The anodic reaction mechanism is more complicated than the cathodic reaction mechanism, especially in mixed acidic solutions. After immersion of the metal (hot rolled steel Fe B500B samples) in the above corrosive water solution, it is soaked with water molecules, which are adsorbed initially in a competitive manner with chlorine ions [52].

The anodic reaction can be described by the following steps:

In the part of anodic surface area where chlorine ions are adsorbed, pitting corrosion is initiated according to equations (24) to (26):

$$Fe + Cl^- + H_2O \leftrightarrow [FeCl(OH)]^-_{ads} + H^+ + e^- \tag{24}$$

$$[FeCl(OH)]^-_{ads} \leftrightarrow FeClOH + e^- \tag{25}$$

$$FeClOH + H^+ \leftrightarrow Fe^{2+} + Cl^- + H_2O \tag{26}$$

In the remaining part of the anodic surface area, the dissolution of iron may occur by the following steps (equations (27) to (29)):

$$Fe + H_2O \leftrightarrow (FeOH)_{ads} + H^+ + e^- \tag{27}$$

$$(FeOH)_{ads} \rightarrow (FeOH)^+ + e^- \tag{28}$$

$$(FeOH)^+ + H^+ \leftrightarrow Fe^{2+} + H_2O \tag{29}$$

When walnut septum extract (WSE) is added to the mixed acidic solution, the corrosion rate of hot rolled steel Fe B500B is inhibited moderately. The inhibition mechanism is explained by the adsorption of compounds contained in the walnut septum extract. Rusu *et al*. [22] reported that the main compounds found in walnut septum extract are phenolic compounds presented in Figure 11. Their HPLC-DAD quantitative analysis of the extract confirmed the presence and the respective concentrations of these main compounds, *i.e.,* gallic acid (7.249 mg L^{-1}); catechin (25.005 mg L^{-1}); isoquercitrin (5.701 mg L^{-1}) and quercitrin (87.520 mg L^{-1}).

These compounds contain many polar groups of oxygen atoms, which can be protonated in the acidic medium according to:

$$WSE + xH^+ \rightarrow WSEH_x^{x+} \tag{30}$$
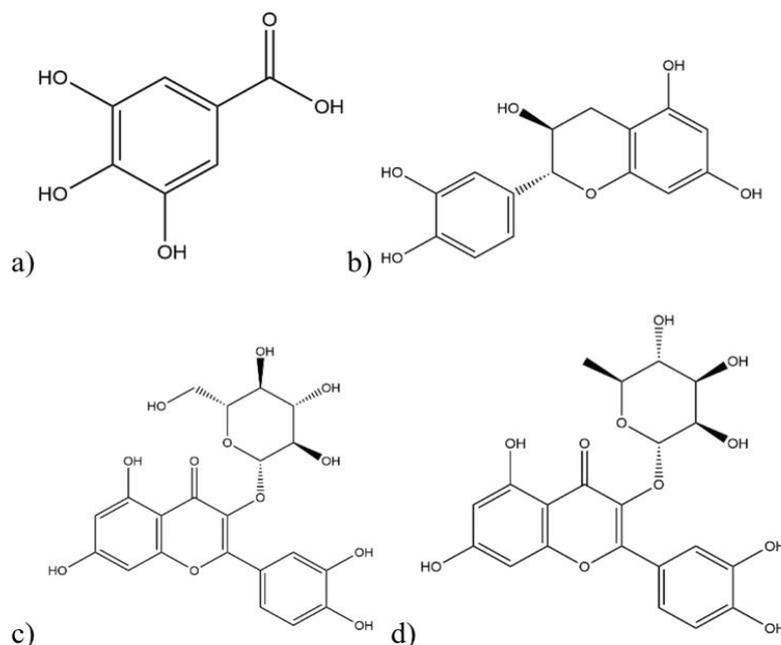
Figure 11. *Main compounds found in walnut septum extract: a) gallic acid, b) catechin, c) isoquercitrin, d) quercitrin*

In mixed acidic solution (0.5 M H_2SO_4/0.5 M HCl), WSE compound exists in two main forms: WSE and $WSEH_x^{x+}$. During the corrosion process of hot rolled steel Fe B500B samples surface would be covered by HSO_4^-, SO_4^{2-} and Cl^- ions (the last one is adsorbed on the surface), converting the surface of the metal from the positively charged into the negatively charged [49].

The physisorption of the WSE occurred between the surface of Fe B500B samples of negatively charged and protonated compounds $WSEH_x^{x+}$. This possibly occurred on the active anodic side of the metal as electrostatic attraction [55].

The chemisorption of the WSE compounds (protonated and unprotonated) occurred on the interface of the cathodic site of the metal surface Fe B500B samples through coordinate bonds and back-donating bonds due to the presence of heteroatoms like oxygen that provide electron lone pairs to the Fe vacant 3d orbitals [55]. The scheme of the suggested adsorption of main inhibitor compounds is shown in Figure 12.
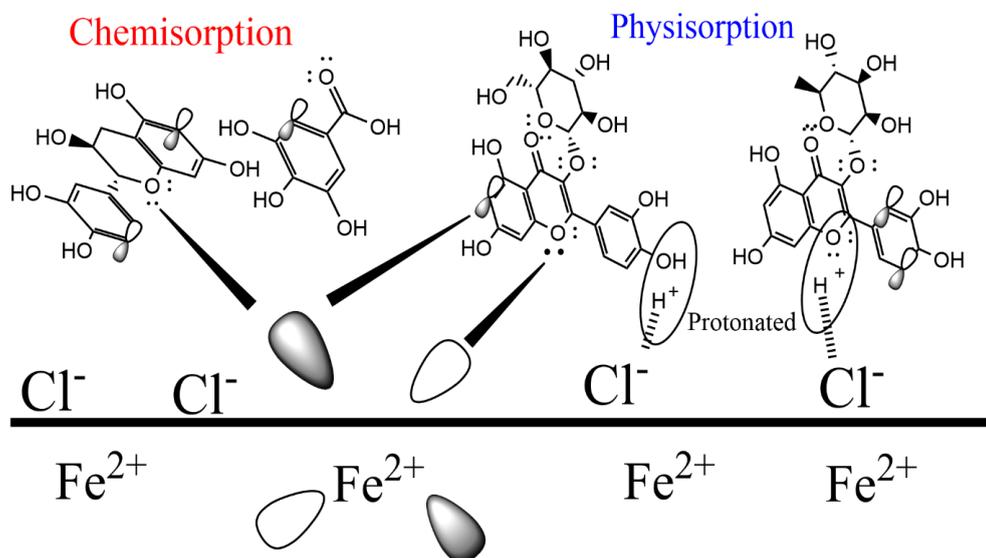
Figure 12. *Suggested mechanism for the adsorption of main compounds of walnut septum extract on Fe B500B samples in mixed acidic solution*

Conclusions

The present work evaluated the inhibition properties of walnut fruit septum alcoholic extract for Fe B500B samples in the presence of the mixed acidic medium (0.5 M H_2SO_4/0.5 M HCl) at temperatures from 298 to 318 K. The inhibitor molecules were easily extracted under reflux. The presence of gallic acid, catechin, isoquercitrin, and quercitrin (suitable for corrosion inhibitors) was qualitatively and quantitatively confirmed by HPLC-DAD spectroscopy. The classical weight loss method results displayed very good performance of the inhibitor at 298 K, reaching a maximum inhibitor efficiency of 79.51 % for 300 mg L^{-1} of the extract added. The adsorption of the inhibitor molecules obeys the Flory-Huggins isotherm that indicated the physisorption on the surface of Fe B500B samples. ATR-FTIR spectra of the Fe B500B in polished form, immersed in the blank and optimum concentration of the inhibitor and pure alcoholic extract, confirmed the presence of phenolic compounds on the surface of the Fe B500B samples, indicating the adsorption of the walnut septum extract molecules on the sample surfaces. The Arrhenius equation displays an endothermic dissolution process at the surface of the Fe B500B samples. The increase in temperature accelerates the corrosion processes, and with the increase of inhibitor concentration at 298 K, the corrosion rates decrease. Potentiodynamic polarization curves displayed inhibition of both anodic and cathodic reactions when increasing the inhibitor concentration. This indicates that the walnut fruit septum extract acts as a mixed-type inhibitor. From the kinetic calculation, inhibition efficiency resulted in 86.99 %. The increase in the temperature decreases the inhibition efficiency. The Nyquist plots present slightly depressed capacitive loops, showing an increase in diameters with an increase of the inhibitor concentration due to an increase of charge transfer resistance, indicating the adsorption of walnut fruit septum extract at the metal solution interface. The charge transfer resistance decreases with the increase in temperature, indicating desorption of the inhibitor molecules. Surface characterization with SEM further confirms the adsorption of the inhibitor molecules on the surface of the Fe B500B samples. This work modestly contributes to more sustainable sources of corrosion inhibition for a safer and cleaner environment.

References

[1] G. Koch, *Cost of corrosion*, in *Trends in Oil and Gas Corrosion Research and Technologies*, A. M. El-Sherik Ed., Woodhead Publishing, Boston, 2017, pp. 3-30. https://doi.org/10.1016/B978-0-08-101105-8.00001-2

[2] C. J. Brown, D. R. Olsen, Regeneration of hydrochloric acid pickle liquors by crystallization, *Iron control technologies: proceedings of the Third International Symposium on Iron Control in Hydrometallurgy*, Montreal, Canada, October 1-4, 2006. ISBN: 189447564X. https://www.yumpu.com/en/document/read/11519218/regeneration-of-hydrochloric-acid-pickle-liquors-by-

[3] M. Abdallah, K. A. Soliman, B. A. Al Jahdaly, J. H. Al-Fahemi, H. Hawsawi, H. M. Altass, M. S. Motawea, S. S. Al-Juaid, Natural parsley oil as a green and safe inhibitor for corrosion of X80 carbon steel in 0.5 M H_2SO_4 solution: a chemical, electrochemical, DFT and MC simulation approach, *RSC Advances* **12 (5)** (2022) 2959-2971. https://doi.org/10.1039/D1RA08855F

[4] M. Abdallah, H. M. Altass, A. S. Al-Gorair, J. H. Al-Fahemi, B. A. A. L. Jahdaly, K.A. Soliman, Natural nutmeg oil as a green corrosion inhibitor for carbon steel in 1.0 M HCl solution:

Chemical, electrochemical, and computational methods, *Journal of Molecular Liquids* **323** (2021) 115036. https://doi.org/10.1016/j.molliq.2020.115036

[5]   L. Chen, D. Lu, Y. Zhang, Organic Compounds as Corrosion Inhibitors for Carbon Steel in HCl Solution: A Comprehensive Review, *Materials* **15(6)** (2022) 2023. https://www.mdpi.com/1996-1944/15/6/2023

[6]   A. Ait Aghzzaf, D. Veys-Renaux, E. Rocca, Pomegranate peels crude extract as a corrosion inhibitor of mild steel in HCl medium: Passivation and hydrophobic effect, *Materials and Corrosion* **71(1)** (2020) 148-154. https://doi.org/10.1002/maco.201911049

[7]   G. I. Ramírez-Peralta, U. León-Silva, M. E. Nicho Díaz, M. G. Valladares-Cisneros, Effect of *Equisetum arvense* extract as corrosion inhibitor of A36 steel in sulfuric acid solution, *Materials and Corrosion* **69(11)** (2018) 1631-1637. https://doi.org/10.1002/maco.201810119

[8]   S. E. Adeniji, B. A. Akindehinde, Comparative analysis of adsorption and corrosion inhibitive properties of ethanol extract of Dialium Guineense leaves for mild steel in 0.5 M HCl, *Journal of Electrochemical Science and Engineering* **8(3)** (2018) 219-226. https://doi.org/10.5599/jese.486

[9]   F. E. Abeng, V. Anadebe, P. Y. Nkom, K. J. Uwakwe, E. G. Kamalu, Experimental and theoretical study on the corrosion inhibitor potential of quinazoline derivative for mild steel in hydrochloric acid solution, *Journal of Electrochemical Science and Engineering* **11(1)** (2020) 11-26. https://doi.org/10.5599/jese.887

[10]   I. H. Ali, A. M. Idris, M. H. A. Suliman, Evaluation of Leaf and Bark Extracts of Acacia tortilis as Corrosion Inhibitors for Mild Steel in Seawater: Experimental and Studies, *International Journal of Electrochemical Science* **14(7)** (2019) 6406-6419. https://doi.org/10.20964/2019.07.10

[11]   H. S. Gadow, M. M. Motawea, Investigation of the corrosion inhibition of carbon steel in hydrochloric acid solution by using ginger roots extract, *RSC Advances* **7(40)** (2017) 24576-24588. https://doi.org/10.1039/C6RA28636D

[12]   K. Hjouji, E. Ech-chihbi, I. Atemni, M. Ouakki, T. Ainane, M. Taleb, Z. Rais, Datura stramonium plant seed extracts as a new green corrosion inhibitor for mild steel in 1M HCl solution: Experimental and surface characterization studies, *Sustainable Chemistry and Pharmacy* **34** (2023) 101170. https://doi.org/10.1016/j.scp.2023.101170

[13]   F. Kaya, R. Solmaz, İ. H. Geçibesler, Investigation of adsorption, corrosion inhibition, synergistic inhibition effect and stability studies of Rheum ribes leaf extract on mild steel in 1 M HCl solution, *Journal of the Taiwan Institute of Chemical Engineers* **143** (2023) 104712. https://doi.org/10.1016/j.jtice.2023.104712

[14]   A. Jano, A. Lame, E. Kokalari, Test of inhibitors for preventing corrosion of steel reinforcement in concrete, *Ovidius University Annals of Chemistry* **32(2)** (2021) 110-113. https://doi.org/10.2478/auoc-2021-0016

[15]   X. Wang, L. Chen, F. Yang, Q. Xiang, J. Liu, Corrosion inhibition mechanism and extraction technology of plant corrosion inhibitors: a review, *Journal of Adhesion Science and Technology* **37(21)** (2023) 2919-2943. https://doi.org/10.1080/01694243.2023.2172993

[16]   M. Abdallah, K. A. Soliman, M. Alfakeer, A. M. Al-bonayan, M. T. Alotaibi, H. Hawsawi, O. A. Hazazi, R. S. Abdel Hameed, M. Sobhi, Mitigation effect of natural lettuce oil on the corrosion of mild steel in sulfuric acid solution: chemical, electrochemical, computational aspects, *Green Chemistry Letters and Reviews* **16(1)** (2023) 2249019. https://doi.org/10.1080/17518253.2023.2249019

[17]   A. R. Shahmoradi, M. Ranjbarghanei, A.A. Javidparvar, L. Guo, E. Berdimurodov, B. Ramezanzadeh, Theoretical and surface/electrochemical investigations of walnut fruit green husk extract as effective inhibitor for mild-steel corrosion in 1M HCl electrolyte,

Journal of Molecular Liquids **338** (2021) 116550.
https://doi.org/10.1016/j.molliq.2021.116550

[18]   M. Okutan, A. Asan, H. E. Singer, The Effect of the Oğuzlar Walnut Extract as a Green
        Corrosion Inhibitor on AISI 1010 Mild, Steel *Hittite Journal of Science and Engineering* **10(1)**
        (2023) 33-41. https://doi.org/10.17350/HJSE19030000288

[19]   S. A. Haddadi, E. Alibakhshi, G. Bahlakeh, B. Ramezanzadeh, M. Mahdavian, A detailed
        atomic level computational and electrochemical exploration of the Juglans regia green fruit
        shell extract as a sustainable and highly efficient green corrosion inhibitor for mild steel in
        3.5 wt% NaCl solution, *Journal of Molecular Liquids* **284** (2019) 682-699.
        https://doi.org/10.1016/j.molliq.2019.04.045

[20]   X. Gu, H. Zhang, Z. Zhang, W. Du, S. Zhu, G. Chen, Modification and Application of Walnut
        Peel Extract as Acidic Corrosion Inhibitor, *Journal of Biobased Materials and Bioenergy*
        15(6) (2021) 820-825. https://doi.org/10.1166/jbmb.2021.2138

[21]   M. Akin, S. Nalbantoglu, O. Cuhadar, D. Uzun, N. Saki, *Juglans regia* L. extract as green
        inhibitor for stainless steel and aluminium in acidic media, *Research on Chemical
        Intermediates* **41(2)** (2015) 899-912. https://doi.org/10.1007/s11164-013-1241-x

[22]   M. E. Rusu, I. Fizesan, A. Pop, A. Mocan, A.-M. Gheldiu, M. Babota, D. C. Vodnar, A. Jurj, I.
        Berindan-Neagoe, L. Vlase, D.-S. Popa, Walnut (*Juglans regia* L.) Septum: Assessment of
        Bioactive Molecules and In Vitro Biological Effects, *Molecules* **25(9)** *(*2020) 2187.
        https://doi.org/10.3390/molecules25092187

[23]   M. E. Rusu, A.-M. Gheldiu, A. Mocan, C. Moldovan, D.-S. Popa, I. Tomuta, L. Vlase, Process
        Optimization for Improved Phenolic Compounds Recovery from Walnut (*Juglans regia* L.)
        Septum: Phytochemical Profile and Biological Activities, *Molecules* **23(11)** (2018) 2814.
        https://doi.org/10.3390/molecules23112814

[24]   S. E. Nataraja, T. V. Venkatesha, K. Manjunatha, B. Poojary, M. K. Pavithra, H. C. Tandon,
        Inhibition of the corrosion of steel in hydrochloric acid solution by some organic molecules
        containing the methylthiophenyl moiety, *Corrosion Science* **53(8)** (2011, 2651-2659.
        https://doi.org/10.1016/j.corsci.2011.05.004

[25]   E. E. El-Katori, S. Al-Mhyawi, Assessment of the *Bassia muricata* extract as a green
        corrosion inhibitor for aluminum in acidic solution, *Green Chemistry Letters and Reviews*
        12(1) (2019) 31-48. https://doi.org/10.1080/17518253.2019.1569728

[26]   A. Khadraoui, A. Khelifa, M. Hadjmeliani, R. Mehdaoui, K. Hachama, A. Tidu, Z. Azari, I.B.
        Obot, A. Zarrouk, Extraction, characterization and anti-corrosion activity of *Mentha
        pulegium* oil: Weight loss, electrochemical, thermodynamic and surface studies, *Journal of
        Molecular Liquids* **216** (2016) 724-731. https://doi.org/10.1016/j.molliq.2016.02.005

[27]   P. Kannan, P. Jithinraj, M. Natesan, Multiphasic inhibition of mild steel corrosion in H$_2$S gas
        environment, *Arabian Journal of Chemistry* **11(3)** (2018) 388-404.
        https://doi.org/10.1016/j.arabjc.2014.10.032

[28]   M. Kaddouri, M. Bouklah, S. Rekkab, R. Touzani, S.S. Al-Deyab, B. Hammouti, A. Aouniti, Z.
        Kabouche, Thermodynamic, Chemical and Electrochemical Investigations of Calixarene
        Derivatives as Corrosion Inhibitor for Mild Steel in Hydrochloric Acid Solution, *International
        Journal of Electrochemical Science* **7(9)** (2012) 9004-9023. https://doi.org/10.1016/S1452-
        3981(23)18047-3

[29]   E.A. Noor, Temperature Effects on the Corrosion Inhibition of Mild Steel in Acidic Solutions
        by Aqueous Extract of Fenugreek Leaves, *International Journal of Electrochemical Science*
        2(12) (2007) 996-1017. https://doi.org/10.1016/S1452-3981(23)17129-X

[30]   C. M. Fernandes, T. da S. Ferreira Fagundes, N. Escarpini dos Santos, T. Shewry de M.
        Rocha, R. Garrett, R. M. Borges, G. Muricy, A. L. Valverde, E. A. Ponzio, *Ircinia strobilina*

crude extract as corrosion inhibitor for mild steel in acid medium, *Electrochimica Acta* **312** (2019) 137-148. https://doi.org/10.1016/j.electacta.2019.04.148

[31] X. Wang, H. Yang, F. Wang, An investigation of benzimidazole derivative as corrosion inhibitor for mild steel in different concentration HCl solutions, *Corrosion Science* **53(1)** (2011) 113-121. https://doi.org/10.1016/j.corsci.2010.09.029

[32] X. Li, X. Xie, S. Deng, G. Du, Two phenylpyrimidine derivatives as new corrosion inhibitors for cold rolled steel in hydrochloric acid solution, *Corrosion Science* **87** (2014) 27-39. https://doi.org/10.1016/j.corsci.2014.05.017

[33] C. Cao, On electrochemical techniques for interface inhibitor research, *Corrosion Science* **38(12)** (1996) 2073-2082. https://doi.org/10.1016/S0010-938X(96)00034-0

[34] Y. Wang, G. Cheng, Y. Li, Observation of the pitting corrosion and uniform corrosion for X80 steel in 3.5wt.% NaCl solutions using in-situ and 3-D measuring microscope, *Corrosion Science* **111** (2016), 508-517. https://doi.org/10.1016/j.corsci.2016.05.037

[35] Y. Qiang, L. Guo, S. Zhang, W. Li, S. Yu, J. Tan, Synergistic effect of tartaric acid with 2,6-diaminopyridine on the corrosion inhibition of mild steel in 0.5 M HCl, *Scientific Reports* **6(1)** (2016) 33305. https://doi.org/10.1038/srep33305

[36] Z. Tao, W. He, S. Wang, G. Zhou, Electrochemical Study of Cyproconazole as a Novel Corrosion Inhibitor for Copper in Acidic Solution, *Industrial & Engineering Chemistry Research* **52(50)** (2013) 17891-17899. https://doi.org/10.1021/ie402693d

[37] T. Vennila, T. Muneeswaran, M. Manjula, B. Stalin, J. Vairamuthu, Synergism between sodium molybdate and binary inhibitor (BHI + Zn^{2+}) on corrosion inhibition of mild steel in aqueous medium containing 60 ppm Cl^- ion, *Materials Research Express* **6(11)** (2019) 1165g6. https://doi.org/10.1088/2053-1591/ab5233

[38] Y. Qiang, S. Zhang, B. Tan, S. Chen, Evaluation of *Ginkgo* leaf extract as an eco-friendly corrosion inhibitor of X70 steel in HCl solution, *Corrosion Science* **133** (2018) 6-16. https://doi.org/10.1016/j.corsci.2018.01.008

[39] P. Du, S. Deng, G. Du, D. Shao, D. Xu, X. Li, Synergistic inhibition effect of *Mikania micrantha* extract with potassium iodide on the corrosion of cold rolled steel in methanesulfonic acid solution, *Corrosion Science* **220** (2023) 111296. https://doi.org/10.1016/j.corsci.2023.111296

[40] G. Sığırcık, D. Yildirim, T. Tüken, Synthesis and inhibitory effect of N,N'-bis(1-phenylethanol)ethylenediamine against steel corrosion in HCl Media, *Corrosion Science* **120** (2017) 184-193. https://doi.org/10.1016/j.corsci.2017.03.003

[41] Q. Wang, R. Wang, X. Sun, R. Aslam, X. Zhou, Q. Zhang, C. Zhao, Y. Sun, Z. Yan, X. Li, Protein-derived carbon dots as green corrosion inhibitors for carbon steel in sulfuric acid solution, *Diamond and Related Materials* **145** (2024) 111135. https://doi.org/10.1016/j.diamond.2024.111135

[42] A. K. Badawi, I. S. Fahim, A critical review on green corrosion inhibitors based on plant extracts: Advances and potential presence in the market, *International Journal of Corrosion and Scale Inhibition* **10(4)** (2021) 1385-1406. https://doi.org/10.17675/2305-6894-2021-10-4-2

[43] A. Miralrio, A. Espinoza Vazquez, Plant Extracts as Green Corrosion Inhibitors for Different Metal Surfaces and Corrosive Media: A Review, *Processes* **8(8)** (2020) 942. https://doi.org/10.3390/pr8080942

[44] A. B. D. Nandiyanto, R. Oktiani, R. Ragadhita, How to read and interpret FTIR spectroscope of organic material, *Indonesian Journal of Science and Technology* **4(1)** (2019) 97-118. http://dx.doi.org/10.17509/ijost.v4i1.15806

[45] D. I. Njoku, Y. Li, H. Lgaz, E. E. Oguzie, Dispersive adsorption of *Xylopia aethiopica* constituents on carbon steel in acid-chloride medium: A combined experimental and

theoretical approach, *Journal of Molecular Liquids* **249** (2018) 371-388. https://doi.org/10.1016/j.molliq.2017.11.051

[46] R. N. Oliveira, M. C. Mancini, F. C. Salles de Oliveira, T. M. Passos, B. Quilty, R. M. da Silva Moreira Thire, G. B. McGuinness, FTIR analysis and quantification of phenols and flavonoids of five commercially available plants extracts used in wound healing, *Revista Matēria* **21(3)** (2016) 767-779. https://doi.org/10.1590/S1517-707620160003.0072

[47] A. Espina, M. V. Cañamares, Z. Jurasekova, S. Sanchez-Cortes, Analysis of iron complexes of tannic acid and other related polyphenols as revealed by spectroscopic techniques: Implications in the identification and characterization of iron gall inks in historical manuscripts, *ACS Omega* **7(32)** (2022) 27937-27949. https://doi.org/10.1021/acsomega.2c01679

[48] N. Errahmany, M. Rbaa, A. S. Abousalem, A. Tazouti, M. Galai, E. H. E. Kafssaoui, M. E. Touhami, B. Lakhrissi, R. Touir, Experimental, DFT calculations and MC simulations concept of novel quinazolinone derivatives as corrosion inhibitor for mild steel in 1.0 M HCl medium, *Journal of Molecular Liquids* **312** (2020) 113413. https://doi.org/10.1016/j.molliq.2020.113413

[49] A. Toghan, H. S. Gadow, H. M. Dardeer, H. M. Elabbasy, New promising halogenated cyclic imides derivatives as potential corrosion inhibitors for carbon steel in hydrochloric acid solution, *Journal of Molecular Liquids* **325** (2021) 115136. https://doi.org/10.1016/j.molliq.2020.115136

[50] P. M. Natishan, E. McCafferty, G. K. Hubler, The Effect of pH of Zero Charge on the Pitting Potential, *Journal of The Electrochemical Society* **133(5)** (1986) 1061. https://doi.org/10.1149/1.2108708

[51] R. G. Pearson, Hard and soft acids and bases, HSAB, part II: Underlying theories, *Journal of Chemical Education* **45(10)** (1968) 643. https://doi.org/10.1021/ed045p643

[52] X. Li, S. Deng, G. Du, X. Xie, Synergistic inhibition effect of walnut green husk extract and sodium lignosulfonate on the corrosion of cold rolled steel in phosphoric acid solution, *Journal of the Taiwan Institute of Chemical Engineers* **114** (2020) 263-283. https://doi.org/10.1016/j.jtice.2020.09.010

[53] S. M. Sayed, H. A. E. Shayeb, The measurement of pitting corrosion currents of steel in neutral aqueous solutions, *Corrosion Science* **28(2)** (1988) 153-162. https://doi.org/10.1016/0010-938X(88)90092-3

[54] K. V. Akpanyung, R. T. Loto, Pitting corrosion evaluation: a review, *Journal of Physics: Conference Series* **1378(2)** (2019) 022088. https://doi.org/10.1088/1742-6596/1378/2/022088

[55] A. Toghan, M. Khairy, M. Huang, A. A. Farag, Electrochemical, chemical and theoretical exploration of the corrosion inhibition of carbon steel with new imidazole-carboxamide derivatives in an acidic environment, *International Journal of Electrochemical Science* **18(3)** (2023) 100072. https://doi.org/10.1016/j.ijoes.2023.100072